LATORY FOR PARTICLE PHYSICS
CERN - SL Division

CERN SL/90-96 (AP)

Bifurcation of the Equilibrium Distribution in Synchrotron Phase Space for Electron Storage Rings with Localized Constant Wake Force.

K. Hirata*, S. Petracca† and F. Ruggiero

Abstract

A simplified mapping is considered which describes the evolution of bunch length and energy spread over one turn for an electron storage ring with localized, constant wake force. This mapping has a period-one fixed point whose stability is investigated analytically. When the period-one fixed point is unstable, a numerical iteration of the mapping reveals the existence of a period-two fixed point. In some case, both types of fixed points can co-exist (bi-stable regime). These results are in good qualitative agreement with those of Multi-Particle Tracking.

Geneva, Switzerland

14 August 1990

*KEK, National Laboratory for High Energy Physics, Tsukuba, Ibaraki 305, Japan.

†On leave of absence from Dipartimento di Matematica e Applicazioni, Universita' di Napoli, Via Mezzocannone 8, 80123 Napoli, Italy.

1 Introduction

The problem of bunch lengthening in electron storage rings has been extensively studied, both analytically and numerically, but several points may still deserve further investigation. Each particle in a bunch is affected by a wake force and, in the conventional analytical theory [1], this force is uniformly distributed along the ring. According to this theory, there exists a threshold current I_{th}, such that if $I < I_{th}$ the bunch distribution is a steady-state solution of the Fokker–Planck equation [2] and satisfies the so-called Potential Well Distortion equation (PWD) [3–5]. Otherwise, if $I > I_{th}$ the static distribution becomes unstable and a regime of 'anomalous bunch lengthening' sets in; then Mode Coupling Theory (MCT) has been used to describe beam instabilities [6–10].

Many of the sources of wake fields should be considered as localized objects and the wake force is therefore a time-dependent function (here time means longitudinal position along the ring). A cluster of several objects (e.g. the RF-cavities of an RF-station) can be further replaced by a single localized source, provided the synchrotron phase advance between the first and the last object be negligible, and such a situation may be more realistic for large machines, such as TRISTAN [11] or LEP [12]. Localized sources of wake fields seem more general, because one can first study the effect of several localized sources and then extend the analysis to the distributed case; the reverse is not true.

A localized wake force is adopted in Multi-Particle Tracking (MPT) [13–16]. Usually this force is applied at one or a few points of the ring, in order to save CPU time. Therefore the conventional analytical theory and MPT are different and it seems desirable to construct an analytic theory which both incorporates the time-dependent wake force and allows the description of unstable regimes. In this paper we discuss a simplified model, where the wake force experienced by the particles is localized at a single point of the storage ring. The distinctive features of our model can be better understood by comparison with those of the conventional analytical theory, that we now shortly review.

The PWD equation governs the steady-state distribution of particles in synchrotron phase space. In the absence of wake fields and for linearized synchrotron oscillations, the particles are confined in a parabolic potential well generated by the RF-voltage and the equilibrium distribution is Gaussian. Wake fields change the shape of the potential well and thus the equilibrium distribution is modified: however, as a consequence of the assumption of distributed wake, this static regime is characterized by a constant energy spread, independent of the beam current. The PWD equation, which is a nonlinear integral equation, has been solved exactly for a purely resistive impedance [17], otherwise only numerical solutions have been presented in the literature [18–21].

To study bunched-beam instabilities several authors [7–9] extended Sacherer's theory. Sacherer used the Vlasov equation, which describes the evolution of the phase-space distribution for proton machines, expressed in polar coordinates. From this equation he derived an integral equation and expanded the solution into azimuthal and radial modes. For low beam intensities [22], the different azimuthal modes are well separated and only coupled-bunch instabilities occur. He extended his theory also to high beam intensities [6], where different azimuthal modes may become coupled, giving rise to a fast instability.

For electron machines, however, the Vlasov equation should be replaced by the Fokker–

Planck equation [2], which includes relaxation effects associated with synchrotron radiation. In the limit where the radiation damping time becomes large and the diffusion constant tends to zero, the Fokker–Planck equation reduces to the Vlasov equation. There are several publications in which the Fokker–Planck equation has been used to try to explain anomalous bunch lengthening (see references in [8]). In particular, Suzuki [9] developed a formalism for solving the Fokker–Planck equation based on Sacherer's theory. He introduced polar coordinates (r, ϕ) in phase space and split the distribution function ψ into two parts: $\psi(r, \phi, t) = \psi_0(r) + \psi_1(r, \phi, t)$. The first part is the stationary solution, neglecting potential well distortion effects, while the second one is a time-dependent perturbation. The Fokker–Planck equation is then linearized with respect to ψ_1 and transformed into an integro-differential equation, azimuthal and radial modes are introduced and the solution is represented through an expansion in terms of generalized Laguerre polynomials. A fast instability occurs when coupling between different azimuthal modes is taken into account. However, he found a discrepancy between theory and experimental data for SPEAR II. As pointed out in a recent paper [23], such a discrepancy may be a consequence of having neglected the effect of the potential well distortion in the stability analysis.

To investigate analytically the consequences of a localized wake source, one of the authors [24] introduced a mapping theory and considered the simplified case where the (short range) longitudinal wake is constant. A non-trivial assumption in this theory is that the distribution function in synchrotron phase space can be approximated by a Gaussian even in presence of wake force. This distribution can thus be parametrized by its first and second order moments alone, describing the barycenter of the beam particles and their spread in synchrotron phase space. The evolution of these moments from turn to turn is governed by a nonlinear mapping, whose period-one fixed point can be found analytically in the case of constant wake. The results obtained in [24], that we summarize and slightly generalize in Sec. 2, show a relatively good agreement with those obtained by MPT and are qualitatively different from those based on PWD. The aim of this paper is to extend the analysis presented in [24], by investigating the stability of the period-one fixed point and revealing some new and perhaps unexpected phenomena.

Within the limits of the Gaussian approximation, the period-one fixed point of the moment mapping is the counterpart of the static solution of the Fokker–Planck equation for a localized wake. In the conventional analytical theory, the Fokker–Planck equation is then linearized around this static solution in order to study its stability against small, time-dependent perturbations. In a similar way, in Sec. 3, we linearize the moment mapping around the period-one fixed point and investigate its stability by looking at the eigenvalues of the corresponding stability matrix. A noticeable difference, however, is that our mapping includes only first and second-order moments of the particle distribution, whereas in MCT the perturbation can be arbitrarily chosen and is usually parametrized by the coefficients of an expansion in a complete basis of orthogonal polynomials.

Corresponding to the unstable character of the period-one fixed point in some region of the parameter space (consisting of synchrotron tune, damping time and normalized strength of the wake force), the results of a numerical iteration of the mapping, presented in Sec. 4, reveal the existence of a period-two fixed point, as well as the possible co-existence

of period-one and period-two solutions, which are both stable.

In order to check the validity of these results, all based on the Gaussian approximation, in Sec. 5 we compare them to the results obtained by Multi-Particle Tracking. The wake force acting on each particle is computed either by an approximate Gaussian fit of the particle distribution or by an exact (but time-consuming) particle-sorting routine. In both cases, the agreement with the analytic results of the stability analysis and with the numerical iteration of the moment mapping is rather good, in spite of the sensible deviations from the Gaussian approximation revealed by MPT. A further check, obtained by the more realistic simulation program SIMTRAC [14], is also quoted.

Finally, in Sec. 6, we briefly discuss the relevance of the present results, together with the assumptions made in our model, to actual storage rings and suggest some possible generalizations and further investigations.

2 The Moment Mapping

The longitudinal beam dynamics in electron storage rings can be described by the stochastic equations of motion for a single particle (Langevin equations). Introducing the normalized synchrotron variables

$$x_1 = \frac{\text{longitudinal displacement}}{\text{natural bunch length}}, \qquad x_2 = \frac{\text{energy deviation}}{\text{natural energy spread}} \tag{2.1}$$

and integrating the Langevin equations over one turn, we obtain the following stochastic mapping valid in the case of localized wake force:

$$\begin{pmatrix} x_1' \\ x_2' \end{pmatrix} = U \begin{pmatrix} x_1 \\ \Lambda x_2 + \hat{r}\sqrt{1-\Lambda^2} - \phi(x_1) \end{pmatrix}, \tag{2.2}$$

where x_1' and x_2' are the synchrotron coordinates after one turn of a particle having initial coordinates x_1 and x_2 just before it experiences the wake force $\phi(x_1)$. Here U is the rotation matrix for synchrotron oscillations with phase advance $\mu = 2\pi\nu$,

$$U = \begin{pmatrix} \cos\mu & \sin\mu \\ -\sin\mu & \cos\mu \end{pmatrix}, \tag{2.3}$$

ν is the synchrotron tune, $\Lambda = \exp(-2/T)$, T is the synchrotron damping time measured in units of the revolution period and $\hat{r}$ a Gaussian random variable with $< \hat{r} >= 0$ and $< \hat{r}^2 >= 1$. Note that synchrotron oscillations have been linearized and are treated in smooth approximation; therefore the integrated effect of radiation over one turn has been localized at a single point of the ring. The wake force $\phi(x_1)$ is given by

$$\phi(x_1) = \frac{eQ}{\sigma_0 E_0} \int_0^\infty \rho(x_1 - u) W(u) du, \tag{2.4}$$

where E_0 is the nominal beam energy, σ_0 the nominal relative energy spread (so that $\sigma_0 E_0$ is the natural energy spread), e denotes the electron charge, Q the total charge in the bunch

and $\rho(x)$ is the charge density normalized to unity. Here $W(u)$ is the longitudinal wake potential (measured in Volt/Coulomb) and represents the voltage induced at a relative distance u behind a unit charge impulse.

The above *stochastic* mapping is equivalent to an infinite hierarchy of *deterministic* mappings for the statistical quantities

$$\begin{aligned} \bar{x}_i &= < x_i >, \\ \sigma_{ij} &= < (x_i - \bar{x}_i)(x_j - \bar{x}_j) >, \\ &\cdots\cdots \end{aligned} \tag{2.5}$$

and so on, which are the moments of the phase-space distribution $\psi(x_1, x_2)$. If ψ is normalized to unity, the average value $< f >$ over all particles of any function $f(x_1, x_2)$ is given by the integral $\int_{-\infty}^{\infty}\int_{-\infty}^{\infty} dx_1 dx_2 \, f\psi$ and the charge density ρ is the integral of ψ over x_2.

The original mapping can be conveniently split into three parts, representing the effect of radiation, wake force and synchrotron oscillation, respectively.

Radiation:

$$\begin{aligned} \bar{x}_1' &= \bar{x}_1 \\ \bar{x}_2' &= \Lambda \bar{x}_2 \\ \sigma_{11}' &= \sigma_{11} \\ \sigma_{12}' &= \Lambda \sigma_{12} \\ \sigma_{22}' &= \Lambda^2 \sigma_{22} + (1 - \Lambda^2) \\ &\cdots\cdots \end{aligned} \tag{2.6}$$

Wake force:

$$\begin{aligned} \bar{x}_1' &= \bar{x}_1 \\ \bar{x}_2' &= \bar{x}_2 - < \phi(x_1) > \\ \sigma_{11}' &= \sigma_{11} \\ \sigma_{12}' &= \sigma_{12} - < (x_1 - \bar{x}_1)\phi(x_1) > \\ \sigma_{22}' &= \sigma_{22} - 2 < (x_2 - \bar{x}_2)\phi(x_1) > + < \phi(x_1)^2 > - < \phi(x_1) >^2 \\ &\cdots\cdots \end{aligned} \tag{2.7}$$

Synchrotron oscillation:

$$\begin{aligned} \bar{x}_i' &= \sum_{j=1}^{2} U_{ij} \bar{x}_j \\ \sigma_{ij}' &= \sum_{h,k=1}^{2} U_{ih} \sigma_{hk} U_{jk} \\ &\cdots\cdots \end{aligned} \tag{2.8}$$

Up to this point, everything is fairly general. In principle, this system should include an infinite number of equations for all higher order moments. We now introduce the main assumption, made in [24], that the distribution function in phase space is always a Gaussian, even in presence of wake force, i.e.

$$\psi(x_1, x_2) = \frac{1}{2\pi\sqrt{\det\ \sigma}} \exp[-\frac{1}{2}\sum_{i,j=1}^{2} \sigma_{ij}^{-1}(x_i - \bar{x}_i)(x_j - \bar{x}_j)]. \tag{2.9}$$

This assumption corresponds to a truncation of the number of equations in the system (2.6), (2.7), (2.8) and in what follows we consider only first and second-order moments. According to the main assumption, the averages in Eq. (2.7) can be calculated as

$$< \phi(x_1) >= \frac{(eQ/\sigma_0 E_0)}{2\sqrt{\pi\sigma_{11}}} \int_0^\infty du\, W(u)\ \exp[-\frac{u^2}{4\sigma_{11}}], \tag{2.10}$$

$$< \phi(x_1)^2 >= \frac{(eQ/\sigma_0 E_0)^2}{2\pi\sqrt{3}\sigma_{11}} \int_0^\infty \int_0^\infty du_1 du_2\, W(u_1)W(u_2)\ \exp[-\frac{u_1^2 + u_2^2 - u_1 u_2}{3\sigma_{11}}], \tag{2.11}$$

$$< (x_1 - \bar{x}_1)\phi(x_1) >= \frac{(eQ/\sigma_0 E_0)}{4\sqrt{\pi\sigma_{11}}} \int_0^\infty du\, u\, W(u)\ \exp[-\frac{u^2}{4\sigma_{11}}], \tag{2.12}$$

$$< (x_2 - \bar{x}_2)\phi(x_1) >= \frac{\sigma_{12}}{\sigma_{11}} < (x_1 - \bar{x}_1)\phi(x_1) > . \tag{2.13}$$

For the sake of simplicity, as in [24], we limit ourselves to the case of a constant wake potential

$$W(u) = \begin{cases} W_0 & , u > 0 \\ 0 & , u \leq 0. \end{cases} \tag{2.14}$$

Then, introducing the dimensionless parameter F_0

$$F_0 = \frac{eQW_0}{\sigma_0 E_0} \tag{2.15}$$

representing the strength of the wake force and proportional to the longitudinal loss factor, Eqs. (2.7) become

$$\begin{aligned} \bar{x}_1' &= \bar{x}_1, \\ \bar{x}_2' &= \bar{x}_2 - \frac{F_0}{2}, \\ \sigma_{11}' &= \sigma_{11}, \\ \sigma_{12}' &= \sigma_{12} - \frac{F_0\sqrt{\sigma_{11}}}{2\sqrt{\pi}}, \\ \sigma_{22}' &= \sigma_{22} - \frac{F_0\sigma_{12}}{\sqrt{\pi\sigma_{11}}} + \frac{F_0^2}{12}. \end{aligned} \tag{2.16}$$

Note that in Eqs. (2.6), (2.16) and (2.8) the barycenter and the moment mappings are decoupled. Generally the barycenter coordinates $\bar{x}_i$ are affected by higher-order moments, but for a constant wake the $\bar{x}_i$ are completely decoupled from them. The second-order moments σ_{ij} are the main subject of our subsequent investigation. Their evolution depends on three parameters: F_0, ν and T.

3 Analytical Investigation of the Stability of the Period-One Fixed Point

The period-one fixed point of the moment mapping, Eqs. (2.6), (2.16) and (2.8), is [24]

$$(\sigma_{11}^{\infty})^{1/2} = -aF_0 + [1 + (a^2 + b)F_0^2]^{1/2}, \tag{3.1}$$

$$\sigma_{12}^{\infty} = \frac{F_0(\sigma_{11}^{\infty})^{1/2}}{2\sqrt{\pi}(1+\Lambda)}, \tag{3.2}$$

$$\sigma_{22}^{\infty} = 1 + F_0^2 \frac{(1-\Lambda^2)\pi - 6\Lambda(1-\Lambda)}{12\pi(1-\Lambda^2)^2}, \tag{3.3}$$

where

$$a = \frac{\cot\mu}{2\sqrt{\pi}(1+\Lambda)}, \tag{3.4}$$

$$b = \frac{\pi(1-\Lambda) + \Lambda(2\pi - 6)}{12\pi(1+\Lambda)(1-\Lambda^2)}. \tag{3.5}$$

In order to investigate the stability of this fixed point, it is convenient to denote by $\vec{\sigma}$ the vector of the second-order moments

$$\vec{\sigma} = \begin{pmatrix} \sigma_{11} \\ \sigma_{12} \\ \sigma_{22} \end{pmatrix}. \tag{3.6}$$

Then the moment mapping can be written as a vector function of $\vec{\sigma}$, i.e.

$$\vec{\sigma}' = \vec{S}(\vec{\sigma}). \tag{3.7}$$

Expanding $\vec{\sigma}$ around the period-one fixed point

$$\vec{\sigma} = \vec{\sigma}^{\infty} + \delta\vec{\sigma}, \tag{3.8}$$

we obtain the linearized mapping

$$\delta\vec{\sigma}' = \underline{\underline{M}}|_{\vec{\sigma}^{\infty}}\, \delta\vec{\sigma}. \tag{3.9}$$

Here the 3×3 stability matrix $\underline{\underline{M}}(\vec{\sigma}, F_0, \nu, T)$ is defined by

$$\underline{\underline{M}} = \frac{\partial\vec{S}}{\partial\vec{\sigma}} \tag{3.10}$$

and has the following form:

$$\underline{\underline{M}} = \begin{pmatrix} \cos^2\mu - \frac{F_0 \sin 2\mu}{4\sqrt{\pi\sigma_{11}}} + \frac{F_0\Lambda\sigma_{12}\sin^2\mu}{2\sigma_{11}\sqrt{\pi\sigma_{11}}} & \Lambda\sin 2\mu - \frac{F_0\Lambda\sin^2\mu}{\sqrt{\pi\sigma_{11}}} & \Lambda^2\sin^2\mu \\ -\frac{\sin 2\mu}{2} + \frac{F_0\Lambda\sigma_{12}\sin 2\mu}{4\sigma_{11}\sqrt{\pi\sigma_{11}}} - \frac{F_0\cos 2\mu}{4\sqrt{\pi\sigma_{11}}} & \Lambda\cos 2\mu - \frac{F_0\Lambda\sin 2\mu}{2\sqrt{\pi\sigma_{11}}} & \frac{\Lambda^2}{2}\sin 2\mu \\ \sin^2\mu + \frac{F_0\sin 2\mu}{4\sqrt{\pi\sigma_{11}}} + \frac{\Lambda F_0\sigma_{12}cos^2\mu}{2\sigma_{11}\sqrt{\pi\sigma_{11}}} & -\Lambda\sin 2\mu - \frac{F_0\Lambda\cos^2\mu}{\sqrt{\pi\sigma_{11}}} & \Lambda^2\cos^2\mu \end{pmatrix}. \tag{3.11}$$

The period-one fixed point is stable if and only if all the (complex) eigenvalues $\lambda_i(\vec{\sigma}^{\infty}, F_0, \nu, T)$, $(i = 1, 2, 3)$, of the matrix $M(\vec{\sigma}^{\infty}, F_0, \nu, T)$ have norm smaller than one. As a matter of fact, if $|\lambda_i| < 1$ for all i, an initial departure $\delta\vec{\sigma}$ from the fixed point solution $\vec{\sigma}^{\infty}$ is damped after iterating the mapping. Conversely, if $|\lambda_i| > 1$ for some i, the initial departure may grow indefinitely.

3.1 Solution of the Secular Equation.

The secular equation for the stability matrix $\underline{\underline{M}}$ can be written as follows:

$$D(\lambda) = \lambda^3 + a_1\lambda^2 + a_2\lambda + a_3 = 0, \tag{3.12}$$

where the real coefficients a_i are complicated functions of the parameters F_0, ν and T. We explicitly computed the eigenvalues (in analytic form) by solving the secular equation for $\underline{\underline{M}}$, which is of third degree in λ, using the well known Cardano formulae [25].

A representative result, for the special cases $\nu = .05, .1, .15$ and $.2$, is shown in Fig. 1, where the black points in the (T, F_0) plane indicate instability of the period-one solution. We call the set of these points the bifurcation area. Obviously, the shape of the bifurcation area depends on the value of the synchrotron tune ν and for larger values of ν, it extends to larger values of the damping time T.

The formulae for the eigenvalues show that they have a complicated dependence on F_0, ν and T, therefore is would be desirable to get some topological information about the bifurcation region in the parameter space. To this end, let us consider the Routh–Hurwitz criterion (see Appendix A), a powerful tool to study the asymptotic stability of a system without explicitly solving the secular equation for the stability matrix. This criterion becomes very useful if we study higher order moments, when the stability matrix has higher dimension and the secular equation cannot be solved analytically.

We can distinguish two classes of systems, with continuous or discrete evolution in time. In the first case the evolution equation is a differential equation and in the second case it is a difference equation, i.e. a mapping. For a system with continuous evolution, the deviations from a steady-state solution obey a linear differential equation associated to a characteristic polynomial $P(s)$, by Laplace transform. The roots $s_k = i\omega_k$ of this polynomial are related to the complex frequencies ω_k of the normal modes and the steady state is asymptotically stable provided all these roots have negative real parts. The Routh–Hurwitz criterion is an algebraic test on the (real) coefficients of the polynomial $P(s)$, allowing to establish whether all its roots lie in the left-half s-plane (see also [26]). For a system with discrete evolution in time, the secular equation $D(\lambda) = 0$ of the linear stability matrix plays the role of the characteristic equation $P(s) = 0$. The stability condition $|\lambda| < 1$ becomes equivalent to $\mathrm{Re}(s) < 0$ under the transformation $s = \frac{\lambda+1}{\lambda-1}$, that associates to the polynomial $D(\lambda)$ a polynomial $P(s)$ whose coefficients are linear combinations of the coefficients of $D(\lambda)$. Thus the Routh–Hurwitz criterion can be easily extended also to discrete-time systems.

Moreover there exists a corollary of Rouché's theorem [27] stating that if the coefficients of a polynomial depend continuously on some real parameters, then the lines $P(i\omega) = 0$ (ω being real), corresponding to purely imaginary roots of the polynomial, divide the parameter space into simply connected, disjoint domains in each of which the polynomial $P(s)$ has a fixed number of zeros with positive real part. Therefore our (F_0, ν, T) space can be divided into disjoint domains, in each of which the period-one fixed point of the moment mapping is either stable or unstable. This helps in the exploration of the parameter space: once a stability boundary is discovered, we know that it must enclose a region where the number of stable and unstable eigenvalues is fixed. Relatively few points are then sufficient to explore the inside of such a region.

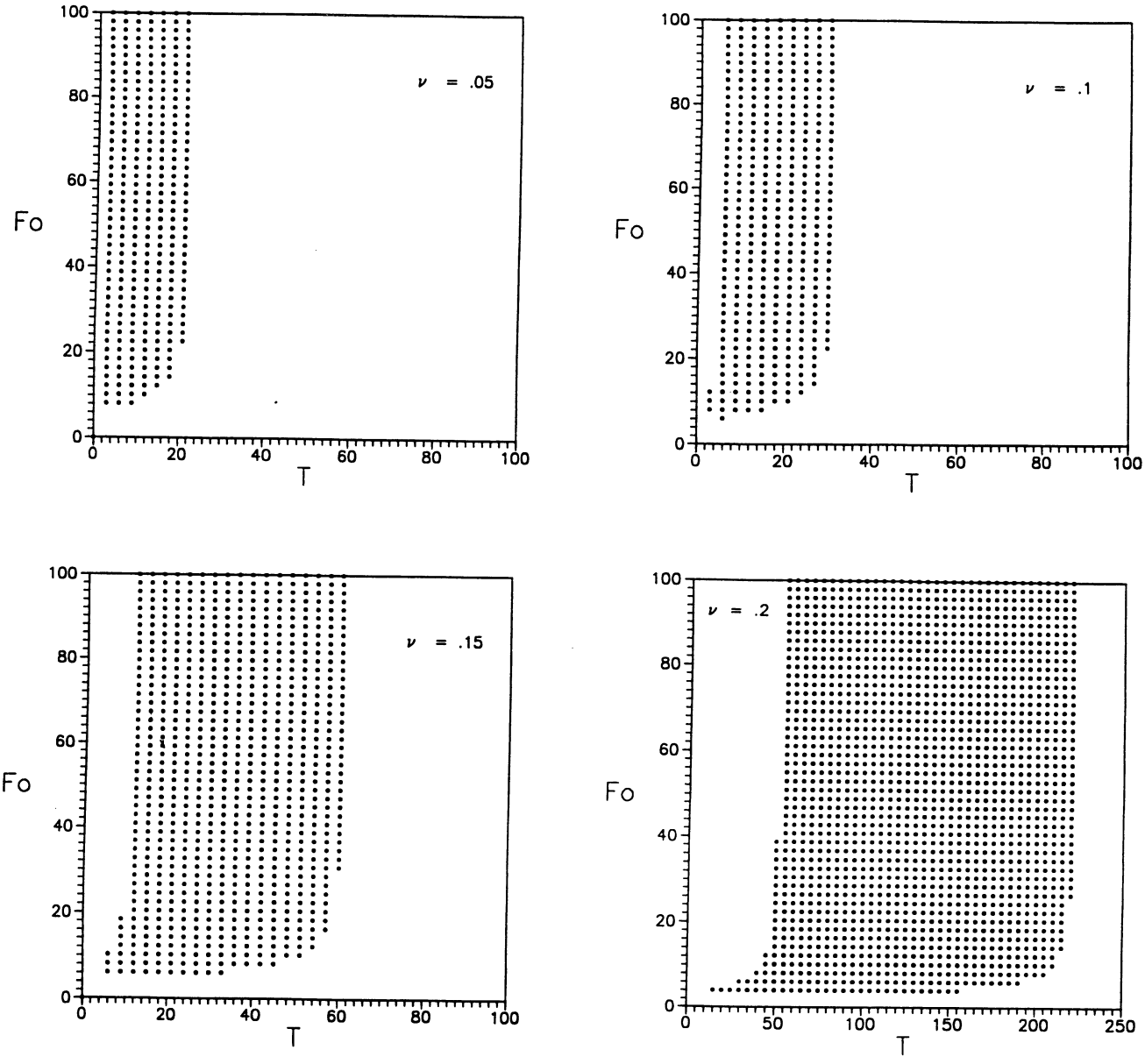

Figure 1: Bifurcation area for $\nu = .05$, $\nu = .1$, $\nu = .15$ and $\nu = .2$.

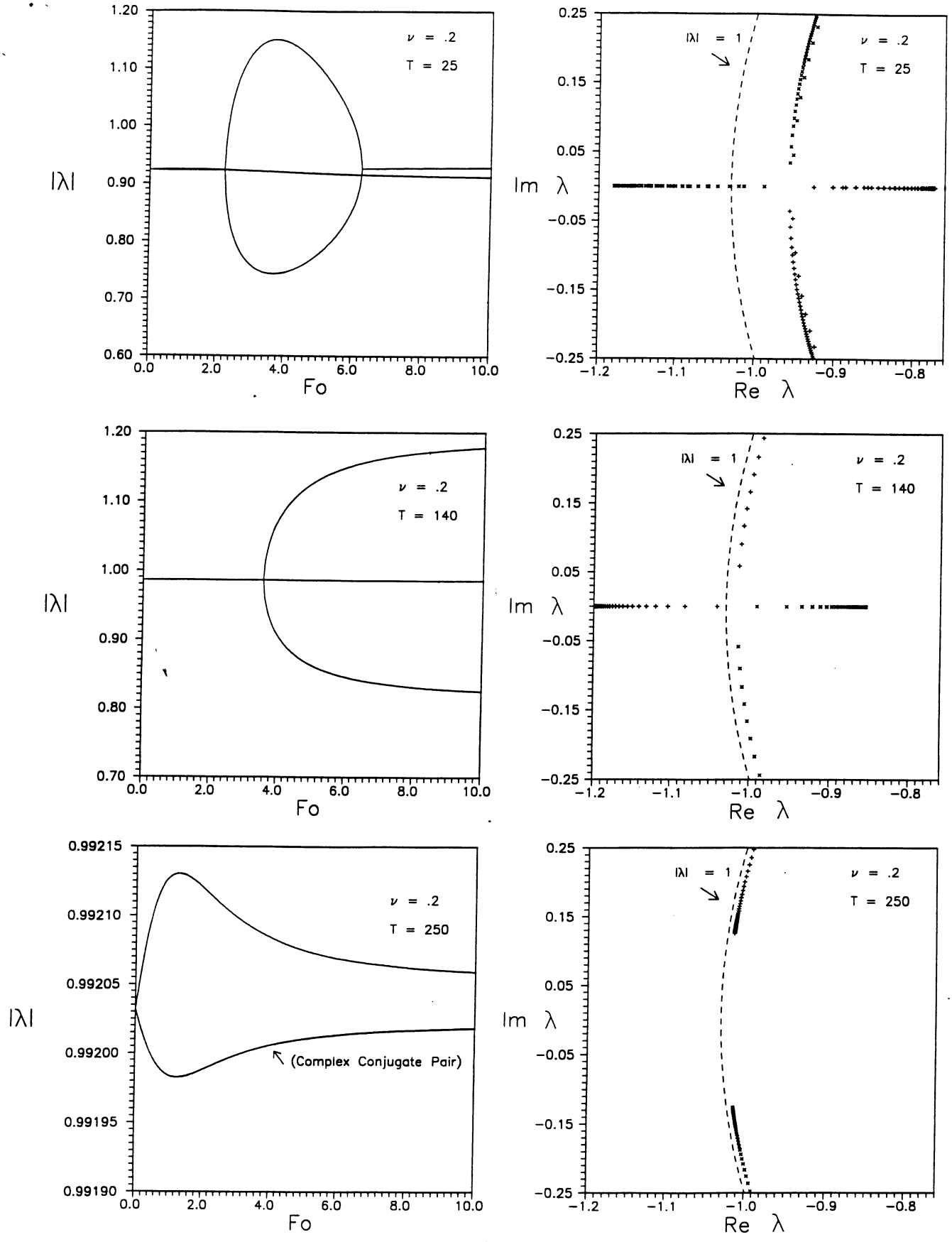

Figure 2: Norms of the eigenvalues vs. F_0 (left) and corresponding trajectories of the eigenvalues in the complex plane (right) for $\nu = .2$ and different values of T.

On the left-hand side of Fig. 2, we plot the eigenvalue norms $|\lambda_i|$, for $\nu = .2$ and different values of T. In the particular case $T = 25$ (top), the period-one fixed point is unstable only in a finite interval of F_0 values. In general, depending on the value of T, the period-one solution can also become definitely unstable above a certain value of F_0, as for $T = 140$ (middle), or remain stable for all F_0 values, as in the bottom plot where T=250.

In the bifurcation regions of Fig. 1, we found that Eq. (3.12) has only one unstable ($|\lambda| > 1$) root. This eigenvalue must be necessarily real, since $D(\lambda)$ is a third degree polynomial with real coefficients, and hence either the roots are all real or two of them are complex conjugate while the third one is real.

On the right-hand side of Fig. 2, we show the eigenvalue trajectories in the complex plane as F_0 changes, for $\nu = .2$ and values of T equal to those of the left-hand side plots. For $T = 25$ (top), one eigenvalue is always real and remains within the unit circle (therefore it is not plotted). The other two are complex conjugate for small F_0. When increasing F_0, they approach the real axis and eventually become real. Then these two roots move in opposite directions along the real axis and, as F_0 enters the unstable range in the left-top picture, one of them crosses the unit circle. Hence, when bifurcation appears, all eigenvalues are real. By further increasing F_0, these two eigenvalues come back and coalesce, within the unit circle, and eventually become again complex conjugate leaving the real axis along paths slightly different from those they came through. This type of behavior is qualitatively similar for all T in the interval from $T \sim 10$ to $T \sim 45$ (for $\nu = .2$).

For values of T such that the period-one solution becomes definitely unstable above a certain value of F_0, the eigenvalue trajectories show the same qualitative behaviour, except that once the complex conjugate pair becomes real, they remain definitely real even increasing F_0, one staying inside the unit circle and the other outside (middle of Fig. 2, where $T = 140$). For values of T such that the period-one solution is stable for all values of F_0, on the other hand, the complex-conjugate pair never reaches the real axis, staying always within the unit circle (see for example the bottom plots of Fig. 2, where $T = 250$).

3.2 Asymptotic Behaviour in Parameter Space.

Here we study the stability of the period-one fixed point for large values of the parameters. Let us consider the limit $F_0 \longrightarrow \infty$ first. Instead of computing

$$\lim_{F_0 \to \infty} \lambda_i(\vec{\sigma}^{\infty}, F_0, \nu, T), \qquad i = 1, 2, 3 \tag{3.13}$$

one can equivalently compute the roots of the secular equation $\det(\underline{\underline{M}}_{F_0 \to \infty} - \lambda\, \underline{\underline{I}}) = 0$, where

$$\underline{\underline{M}}_{F_0 \to \infty} = \lim_{F_0 \to \infty} \underline{\underline{M}}(\vec{\sigma^{\infty}}, F_0, \nu, T). \tag{3.14}$$

The analytic expression of this matrix is reported in Appendix B, together with the corresponding asymptotic expression of the period-one fixed point.

It is seen that the $\sigma^{\infty}_{ij,F_0 \to \infty}$ are proportional to F_0^2 and, since the matrix elements in Eq. (3.11) contain only the ratios $F_0/\sqrt{\sigma_{11}}$ and σ_{12}/σ_{11}, they become independent of F_0. Therefore, for $F_0 \longrightarrow \infty$ the eigenvalues of the stability matrix remain finite. Nevertheless,

the asymptotic values of the $|\lambda_i|$ may still be larger than one: this happens, for example, for the bifurcation regions of Fig. 1.

Similarly for $T \longrightarrow \infty$, i.e. $\Lambda \rightarrow 1$, one easily obtains the asymptotic expression of the stability matrix and of the period-one fixed point (see Appendix B). In this case the stability matrix does not depend on $\vec{\sigma}^{\infty}$, Λ or F_0, so that the eigenvalues are asymptotically functions of ν alone. One of them tends to 1 and the remaining two tend to the complex conjugate pair $\exp(\pm 4\pi i\nu)$: of course, since we are considering the limit of large damping time, the norm of the three eigenvalues tends to unity. However, a numerical investigation of the eigenvalue norms beyond the parameter range of Fig. 1 indicates that no further bifurcation regions appear for larger values of T.

4 Numerical Iteration of the Moment Mapping: Search of Period-Two Fixed Points

In order to further clarify the results of our analytic investigation, we implemented a numerical code which iterates the moment mapping (2.6), (2.16), (2.8). As a result, we found that in the range of parameters where the period-one fixed point is unstable, period-two solutions develop, which are fixed points of

$$\vec{\sigma} = \vec{S}[\vec{S}(\vec{\sigma})]. \tag{4.1}$$

Period-two solutions obviously occur in alternating pairs, $\vec{\sigma}_a^{\infty}, \vec{\sigma}_b^{\infty}$, related by

$$\vec{\sigma}_{a,b}^{\infty} = \vec{S}(\vec{\sigma}_{b,a}^{\infty}). \tag{4.2}$$

This scenario (instability of the period-one solution, onset of a stable period-two solution) is, to the best of our knowledge, completely new for this simple model.

Corresponding to the situation sketched in the top of Fig. 2, we found that period-one and period-two fixed points can co-exist for values of F_0 beyond the region of instability of the period-one solution, each fixed point being an attractor. Therefore a bistable regime shows up and the final fixed point to which the iteration converges depends on the choice of initial conditions. Such a bistable behaviour is encountered quite often, e.g., within the interval from $T \sim 10$ to $T \sim 45$, for $\nu = .2$ (see Fig. 1). This situation is represented in the left-hand side of Fig. 3 with reference to σ_{11}, σ_{12}, σ_{22}, respectively, for $T = 25$. These plots should be compared to those corresponding to the definitely unstable case (see right-hand side of Fig. 3, where $T = 140$) and to the stable case (see Fig. 4, where $T = 250$).

The possibility of bistability should be taken into account even in the conventional analytical theory of anomalous bunch lengthening, since the stability of the static solution of the PWD equation does not rule out the appearance of other time-dependent, stable solutions.

5 Multi-Particle Tracking

The possible dependence of the new results presented above on the Gaussian approximation was checked using a suitable version of Multi-Particle Tracking code, which is based on

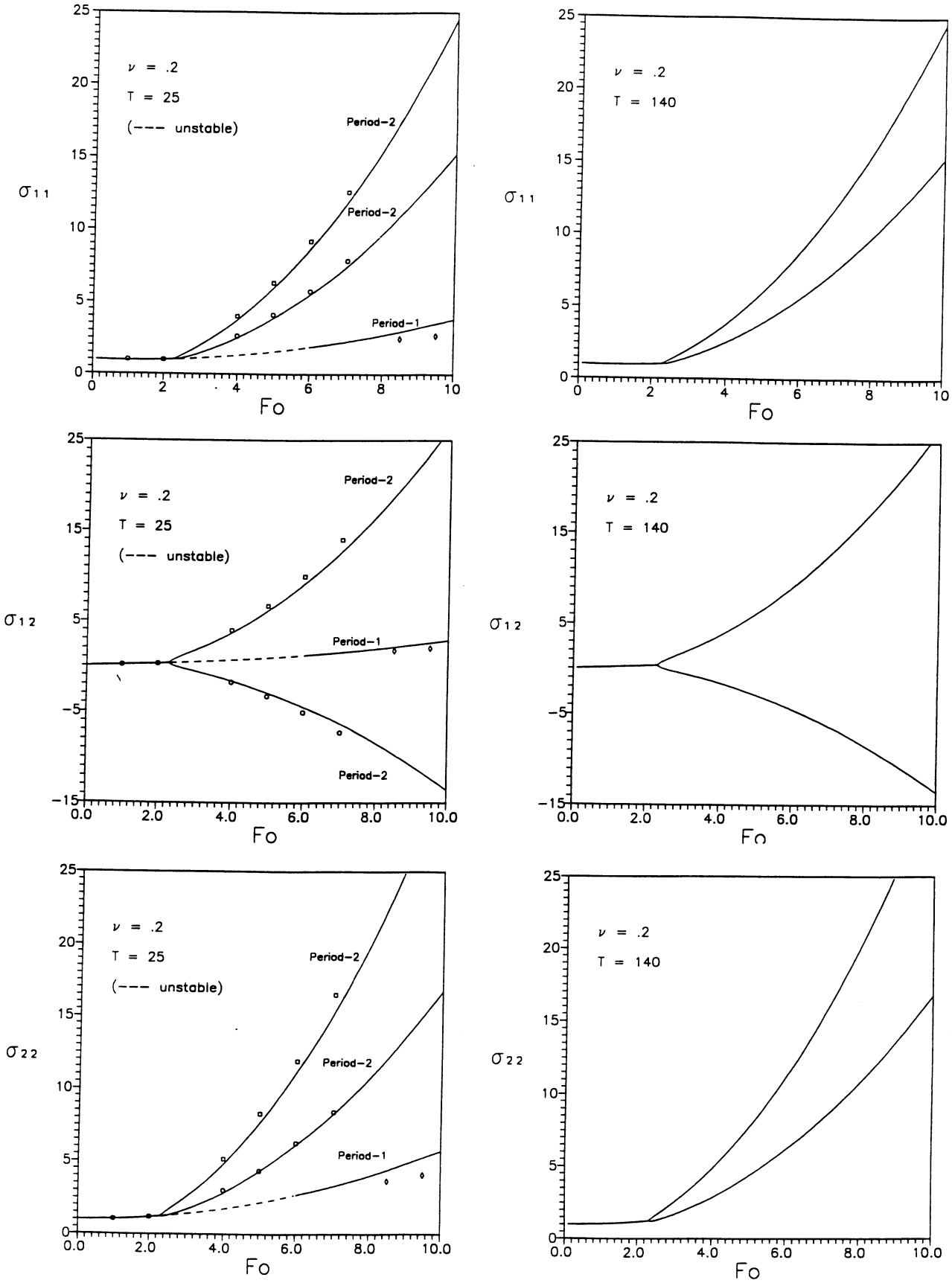

Figure 3: σ_{ij} vs. F_0, for $\nu = .2$ and $T = 25$ (left) or $T = 140$ (right), from numerical iteration of the mapping. Additional symbols in the left-hand side plots indicate the results of MPT (sorting).

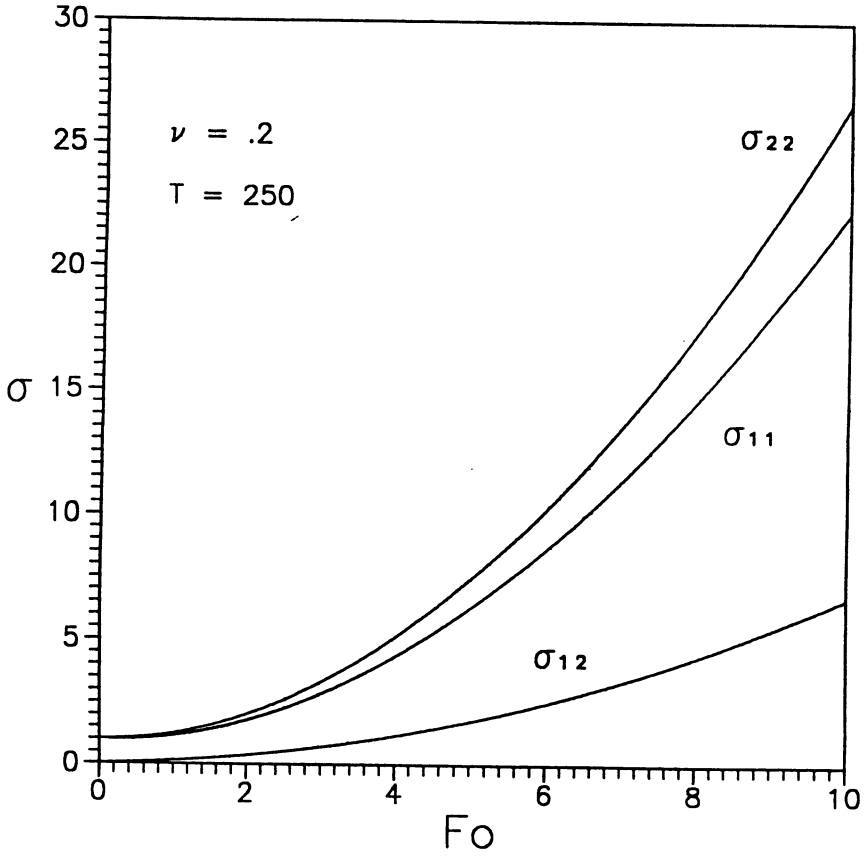

Figure 4: σ_{ij} vs. F_0, for $\nu = .2$ and $T = 250$, from numerical iteration of the mapping.

an entirely different philosophy and has been widely used to study several longitudinal as well as transverse effects in particle accelerators.

In a first version of our code, the stochastic Langevin equations are solved using a Gaussian fit of the particle distribution to compute the wake force acting on each particle. We apply the transformation (2.2) to the phase-space coordinates of an ensemble of 2000 particles. In doing so, the stochastic variable $\hat{r}$ is generated starting from a very good random uniform deviate generator, due to Knuth [28], followed by an elementary transformation to normal deviate, also taken from [28]. The wake force (2.4) is computed assuming a constant wake potential and a Gaussian fit for the charge density $\rho(x)$, computed as

$$\rho(x) = \int_{-\infty}^{+\infty} \psi(x,y)\ dy, \tag{5.1}$$

with $\psi(x,y)$ given by Eq. (2.9), wherein the moments σ_{ij} and the mean values $\overline{x}_i$ are computed according to Eqs. (2.5) and the averages are taken over the particle sample.

In a second version of the code, we use a sorting routine (without binning) to compute the wake force on each particle. An indexing routine is used to enqueue all particles following a given one, in order to compute the wake force from the wake potential, assumed constant. In both cases, the initial particle coordinates in synchrotron phase space are generated as random Gaussian.

The comparison of MPT results with the results of the moment mapping shows a quite satisfactory qualitative/quantitative agreement, including period-doubling and bistability. For the period-two solutions, we also found an unexpected phenomenon: particles tend to cluster into several 'islands' in phase space, possibly related to multipole resonances.

In Fig. 5 we report the results of MPT after 2000 turns, using 2000 particles, with $T = 25$, $\nu = .2$ and $F_0 = 4$. In the case of Gaussian fit (left), besides the core of the bunch distribution one can distinguish four islands. At each turn, only two of them are populated while the other two are almost empty. The island population is reversed at the next turn and the original distribution is recovered after two turns. In the case of MPT with sorting routine (right-hand side of Fig. 5), the islands are less pronounced and the agreement with the results of the moment mapping are even better (see the left-hand side plots of Fig. 3).

By means of a standard contour-plot generating utility, we obtained from Figs. 5 the contour levels shown in Figs. 6. From these plots one can draw the conclusion that the Gaussian approximation for the phase-space distribution function, though allowing to predict the qualitative features of the bunch dynamics, is *not* realistic, in view of the appearance of several maxima.

As a final check of our results, we used the more realistic simulation program SIMTRAC [14]. The latter can track longitudinal as well as transverse motion of a given number of super-particles in a circular machine. The machine geometry is modelled by a ring divided into sectors, each possessing an RF-station and an arc-section, and the synchrotron tune for small amplitude oscillations is controlled by the peak value of a sinusoidal RF-voltage (i.e. synchrotron oscillations are nonlinear and are not treated in smooth approximation). It is possible to assign different values to various parameters and to choose among different wake

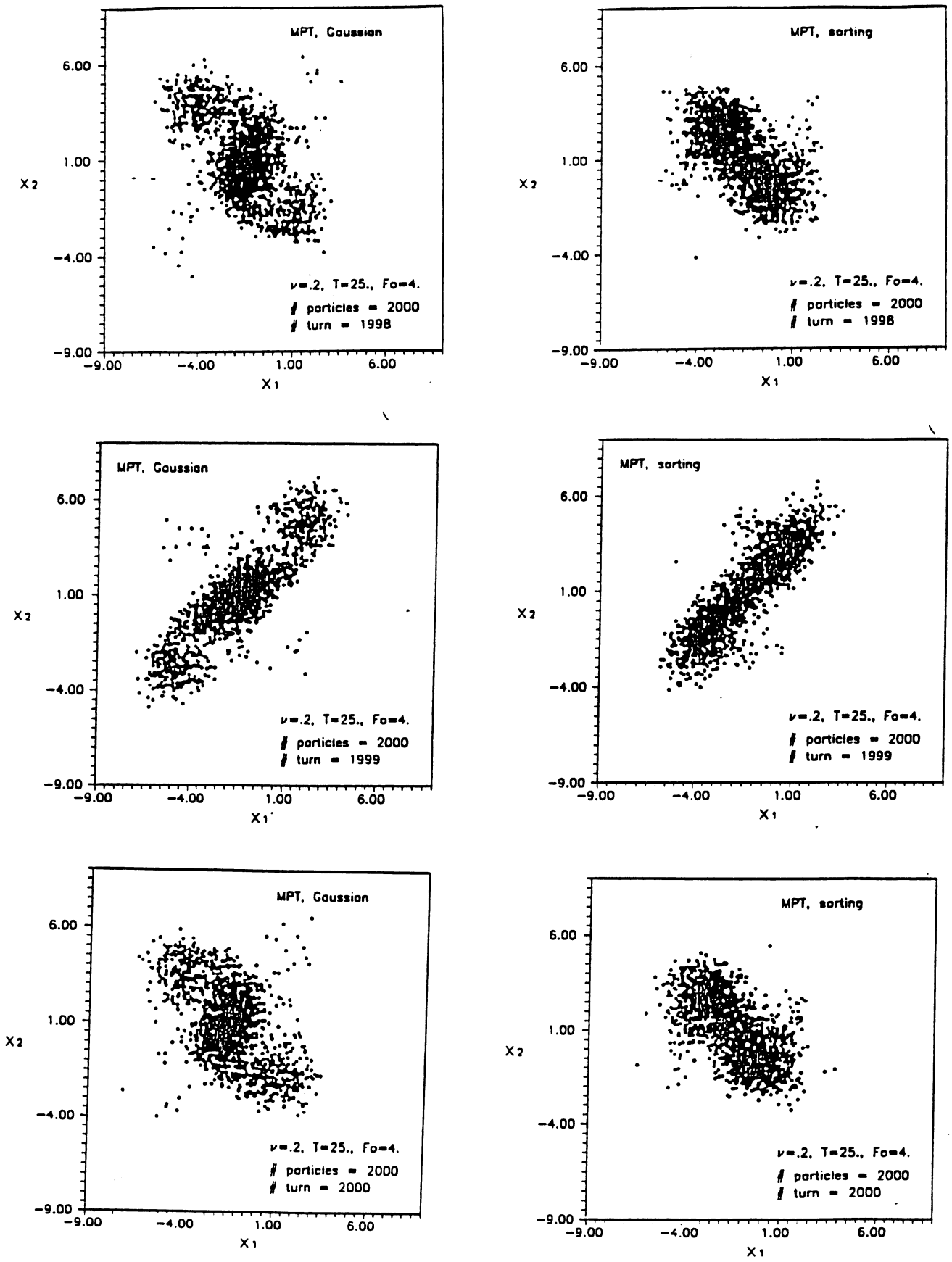

Figure 5: Phase space distribution from MPT, either with Gaussian fit (left) or with sorting routine (right).

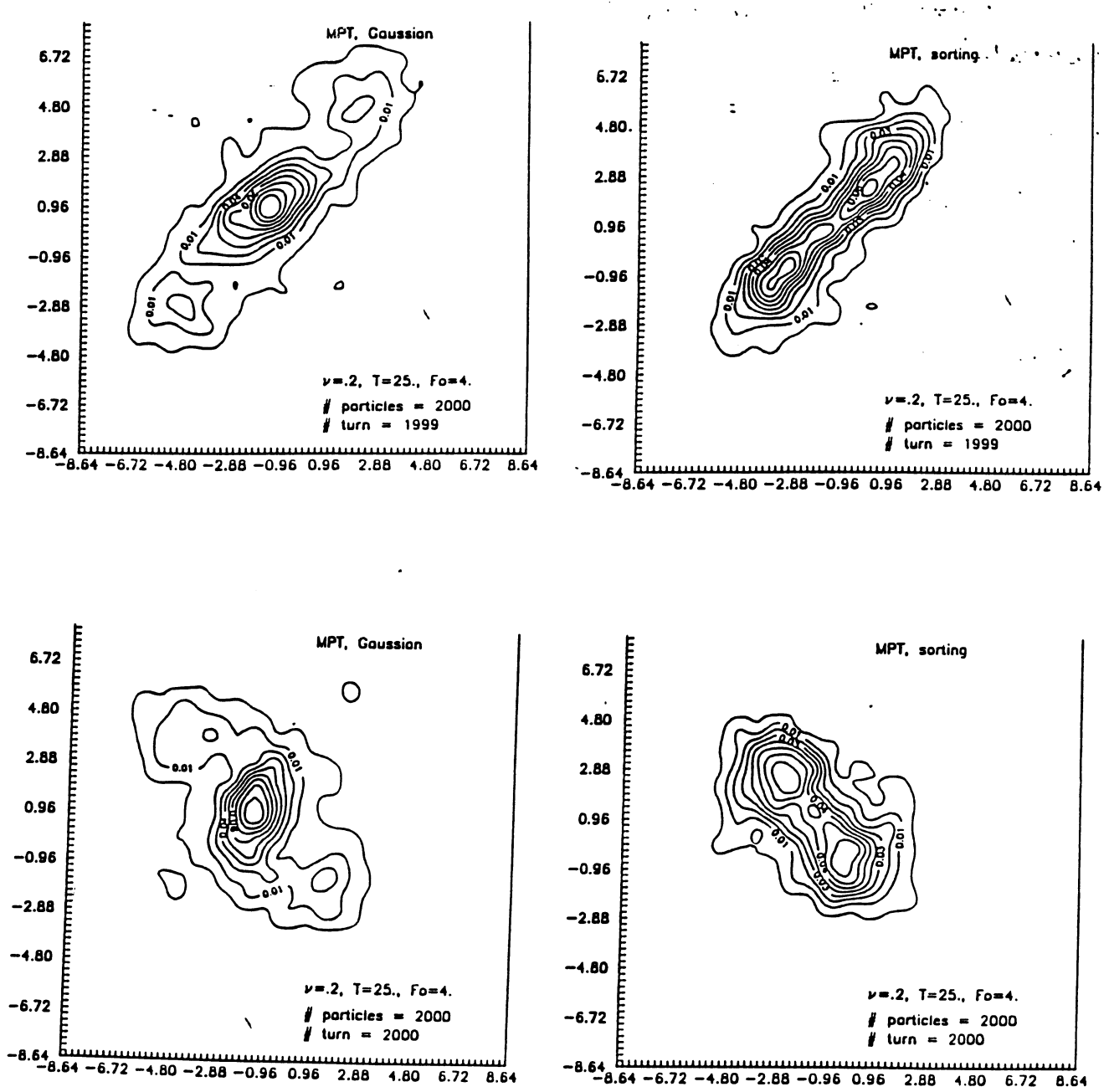

Figure 6: Distribution function contour plots corresponding to Fig. 5.

models. We tracked 500 particles (no binning) with a choice of parameters corresponding to $\nu = .2$, $T = 22$, F_0 around 4 and of course a constant longitudinal wake. The result was in good qualitative agreement with our previous analysis, showing a time-dependent behaviour of the particle distribution even after 400 turns (i.e. more than 18 damping times), with a periodicity of two turns.

6 Discussion and Conclusions

We presented an analytic parametric study of a simplified mapping and the results of its numerical iteration, showing the bifurcation of the equilibrium distribution in synchrotron phase space for electron storage rings with localized, constant wake force, as well as the possible occurrence of bistability. These results have been confirmed by Multi-Particle Tracking. It is reasonable to expect that our model will either show a cascaded period-doubling-bifurcation route to chaos (to be identified with turbulent bunch lengthening) or a back-bifurcation from period-two to period-one solutions, possibly depending on the parameter values. In order to clarify this issue, we hope to extend our analytic approach to discuss the stability of period-two fixed points.

Let us remark that, within the limits of the Gaussian approximation, our moment mapping describes the single-turn *dynamics* of the bunch. This should be contrasted with other bifurcating sequences, discussed in the literature in connection with the PWD equation [29]. Strictly speaking, these bifurcations concern only the iterative solution of a *static* problem, although it is conceivable to attach some dynamical meaning to the iteration procedure.

In the following, we discuss two critical points of our model, namely the assumption of a constant wake and the Gaussian approximation, which help making an analytic approach viable. In connection with the first issue, it should be clearly stated that our model is not realistic, since the wake potential $W(u)$ at a longitudinal distance u behind a unit charge impulse is usually a rapidly decreasing function near the origin and, further behind, it has a damped oscillating behaviour. The first zero of the wake occurs at a distance which depends on the dimensions of the source (e.g. the length of an RF-cavity). When the bunch is much longer then the region of divergence of the wake (typically a few millimeters) and, at the same time, much shorter then the distance of its first zero (typically more than 10 cm), then for most of the particles the wake might be loosely approximated by a constant. However, the dynamical consequences of the divergent part of the wake are difficult to assess, in view of the continuous redistribution of particles within the bunch due to synchrotron oscillations.

The constant wake W_0 appearing in our model should be identified with twice the value of the longitudinal loss factor. In the case of LEP [12], for a bunch length of 1.5 cm this gives $W_0 \sim 550$ V/pC. At injection energy, when $E_0 = 20$ GeV and the relative energy spread is $\sigma_0 \sim 3 \times 10^{-4}$, a bunch current around 0.1 mA (i.e. a total charge in the bunch $Q \sim 10$ nC) corresponds to a normalized strength of the wake force $F_0 \sim 1$. Larger values of F_0 may be reached when approaching the nominal bunch current of 0.75 mA. For reasonable values of the synchrotron tune ν, the range of damping time T in which

our model predicts the instability of the period-one fixed point does not extend beyond a few hundred turns (see Fig. 1). Although such small values of T are typical for LEP at 50 GeV, the corresponding strength F_0 of the wake force scales as the inverse square of the energy E_0 (because of the energy spread $\sigma_0 E_0$ in the denominator of Eq. (2.15)) and thus becomes smaller then unity in the interesting range of bunch current. The situation is even worse at injection energy, when the synchrotron damping time becomes of the order of a few thousands turns. In both cases, as a consequence of the assumption of constant wake, our model predicts an instability threshold much higher than the observed one (around 0.1 mA at 20 GeV [30]).

The other main assumption we made is that the particle distribution in synchrotron phase space can be approximated by a Gaussian, even in presence of wake fields. The results obtained by the correspondingly truncated moment mapping obviously depend on this approximation and, when we compare them to MPT results, it appears that we introduce some unphysical features in our solution, as already noted in [24]. For example, Fig. 6 (left) shows contour plots for the particle distribution corresponding to the period-two fixed point, obtained by MPT with a Gaussian fit for the wake force; the presence of islands in phase space indicates deviations from the Gaussian approximation. In the right-hand side plots of Fig. 6, we use a version of MPT with sorting routine to compute the wake force acting on each particle, which gives the most realistic simulation, and again we see islands in phase space which cannot correspond to a Gaussian distribution. Nevertheless, all the qualitatively new results derived by the moment mapping (period-two solutions and bistability) are confirmed by MPT, especially when the sorting routine is adopted. What we can argue is that, within the Gaussian approximation, we are able to see at least a part of the total number of the system instabilities, which could be described through a more general analytic representation.

In order to improve our model, we plan to consider a more general wake potential (e.g., a superposition of Gauss-Hermite functions) and a Stratonovich expansion of the phase-space distribution as in [31]. The latter allows the introduction of higher-order moments of the particle distribution, although the manipulation of analytic expressions may become very cumbersome (for example, the dimension of the stability matrix tends to infinity).

Acknowledgements

The authors would like to thank B. Zotter and E. Keil for useful comments and discussions. In particular, B. Zotter introduced them to the program SIMTRAC. A special thank goes also to E. Picasso and G. Plass for their encouragement and support. Finally K.H. and S.P. would like to thank all the members of the LEP Theory group for their hospitality and help.

Appendix A Routh–Hurwitz Algorithm

The necessary and sufficient condition for the asymptotic stability of a linear, continuous-time system is that all the zeros of its characteristic polynomial $P(s)$ have negative real parts. A polynomial with this property is called a Hurwitz polynomial. The Routh–Hurwitz algorithm is a powerful tool for discussing asymptotic stability without actually calculating the roots of $P(s)$. The RH algorithm, in its simplest version [32], is embodied in the following

Theorem 1 - *The necessary and sufficient conditions for a polynomial $P(s)$ with real coefficients*

$$P(s) = s^k + b_1 s^{k-1} + ... + b_k$$

to be a Hurwitz polynomial are either

$$b_1 > 0, b_3 > 0, b_5 > 0, ...$$

$$P_2 > 0, P_4 > 0, P_6 > 0, ...$$

or

$$b_2 > 0, b_4 > 0, b_6 > 0, ...$$

$$P_1 > 0, P_3 > 0, P_5 > 0, ...$$

where P_i are the following determinants:

$$P_1 = b_1, P_2 = \begin{vmatrix} b_1 & b_3 \\ 1 & b_2 \end{vmatrix}, P_3 = \begin{vmatrix} b_1 & b_3 & b_5 \\ 1 & b_2 & b_4 \\ 0 & b_1 & b_3 \end{vmatrix}, ...$$

By a suitable modification of the Routh–Hurwitz algorithm for continuous-time systems, it is possible to investigate the stability of discrete-time systems as well. For discrete-time systems, the unit circle in the λ-plane plays the same role as the left-half s-plane for continuous-time systems and the asymptotic stability problem corresponds to determining whether the zeros of a given polynomial

$$D(\lambda) = \lambda^k + a_1 \lambda^{k-1} + a_2 \lambda^{k-2} + ... + a_k$$

lie inside or outside the unit circle.

The bilinear transformation

$$s = \frac{\lambda + 1}{\lambda - 1}$$

maps the interior (exterior) of the unit circle in the λ-plane into the left (right) half s-plane. Hence the zeros of

$$\Delta(s) = D(\frac{s+1}{s-1}) = \frac{P(s)}{(s-1)^k}$$

in the right-half s-plane correspond to the zeros of $D(\lambda)$ outside the unit circle in the λ-plane. The zeros of $\Delta(s)$ are those of its numerator $P(s)$

$$P(s) = b_0 s^k + b_1 s^{k-1} + ... + b_k,$$

hence the stability of the discrete-time system can be discussed by applying the Routh–Hurwitz test to $P(s)$ above.

The coefficients b_i of $P(s)$ are linear combinations of the coefficients a_i of the original polynomial $D(\lambda)$:

$$\begin{pmatrix} b_0 \\ b_1 \\ . \\ . \\ b_k \end{pmatrix} = \underline{\underline{M_k}} \begin{pmatrix} 1 \\ a_1 \\ . \\ . \\ a_k \end{pmatrix}.$$

For the special case of our interest, $k = 3$, the transformation matrix is

$$\underline{\underline{M_3}} = \begin{pmatrix} 1 & 1 & 1 & 1 \\ 3 & 1 & -1 & -3 \\ 3 & -1 & -1 & 3 \\ 1 & -1 & 1 & -1 \end{pmatrix}.$$

Appendix B Asymptotic Formulae

From Eqs. (3.1)–(3.5), the asymptotic expression for the period-one fixed point when $F_0 \longrightarrow \infty$ is the following:

$$\begin{aligned} \sigma^{\infty}_{11,F_0\to\infty} &\sim F_0^2(-a + \sqrt{a^2+b})^2, \\ a &= \frac{\cot\mu}{2\sqrt{\pi}(1+\Lambda)}, \\ b &= \frac{\pi(1-\Lambda) + \Lambda(2\pi - 6)}{12\pi(1+\Lambda)(1-\Lambda^2)}, \\ \sigma^{\infty}_{12,F_0\to\infty} &\sim \frac{F_0\sqrt{\sigma^{\infty}_{11}}}{2\sqrt{\pi}(1+\Lambda)}, \\ \sigma^{\infty}_{22,F_0\to\infty} &\sim \frac{F_0^2((1-\Lambda^2)\pi - 6\Lambda(1-\Lambda))}{12\pi(1-\Lambda^2)^2}. \end{aligned}$$

Then, using Eq. (3.11), the stability matrix $M_{F_0\to\infty}$ has the form

$$M_{F_0\to\infty} \sim \begin{pmatrix} \cos^2\mu - \frac{\sin 2\mu}{4\sqrt{\pi\gamma}} + \frac{\Lambda\sin^2\mu}{4\pi(1+\Lambda)\gamma} & \Lambda\sin 2\mu - \frac{\Lambda\sin^2\mu}{\sqrt{\pi\gamma}} & \Lambda^2\sin^2\mu \\ -\frac{\sin 2\mu}{2} + \frac{\Lambda\sin 2\mu}{8\pi(1+\Lambda)\gamma^2} - \frac{\cos 2\mu}{4\sqrt{\pi\gamma}} & \Lambda\cos 2\mu - \frac{\Lambda\sin 2\mu}{2\sqrt{\pi\gamma}} & \frac{\Lambda^2\sin 2\mu}{2} \\ \sin^2\mu + \frac{\sin 2\mu}{4\sqrt{\pi\gamma}} + \frac{\Lambda\cos^2\mu}{4\pi(1+\Lambda)\gamma^2} & -\Lambda\sin 2\mu - \frac{\Lambda\cos^2\mu}{\sqrt{\pi\gamma}} & \Lambda^2\cos^2\mu \end{pmatrix},$$

with

$$\gamma = -a + \sqrt{a^2 + b}.$$

In the other asymptotic case, $T \longrightarrow \infty$, which means $\Lambda \longrightarrow 1$, the period-one fixed point is

$$\begin{aligned}
\sigma^{\infty}_{11,T\to\infty} &\sim F_0^2 b, \\
\sigma^{\infty}_{12,T\to\infty} &\sim \frac{F_0\sqrt{\sigma^{\infty}_{11}}}{4\sqrt{\pi}}, \\
\sigma^{\infty}_{22,T\to\infty} &\sim 1 + F_0^2 b, \\
b &\sim \frac{\pi - 3}{24\pi(1-\Lambda)},
\end{aligned}$$

while the stability matrix has the following expression:

$$M_{T\to\infty} \sim \begin{pmatrix} \cos^2\mu & \sin 2\mu & \sin^2\mu \\ -\frac{\sin 2\mu}{2} & \cos 2\mu & \frac{\sin 2\mu}{2} \\ \sin^2\mu & -\sin 2\mu & \cos^2\mu \end{pmatrix}.$$

The eigenvalues of this matrix are 1 and $e^{\pm 2i\mu}$.

References

[1] A.W. Chao, SLAC-PUB 2946 (1982).

[2] E. Picasso, L. Radicati and F. Ruggiero, Proc. Joint US-CERN School on Particle Accelerators, Santa Margherita di Pula, Sardinia, 1985, ed. J.M. Jowett, M. Month and S. Turner (Lecture Notes in Physics, **247**, Springer-Verlag, Berlin, 1986), p. 1.

[3] J. Haissinski, Nuovo Cimento **18B**, 72 (1973).

[4] H.G. Hereward, PEP Note 53 (1973).

[5] A. Renieri, LNF-75/11R (1975).

[6] F. Sacherer, IEEE Trans. Nucl. Sci. **NS-24**, 1393 (1977).

[7] G. Besnier, Nucl. Instrum. Methods **164**, 235 (1979).

[8] T. Suzuki, Y. Chin and K. Satoh, Part. Acc. **13**, 179 (1983).

[9] T. Suzuki, Part. Acc. **14**, 91 (1983).

[10] Y. Chin and K. Yokoya, Nucl. Instrum. Methods **226**, 223 (1984).

[11] K. Nakajima and A. Ogata, 6th Symp. on Acc. Science and Technology, 1987, Tokyo, Japan (IONICS, Tokyo, 1987).

[12] I. Wilson and H. Henke, CERN Report 89-09 (1989).

[13] T. Weiland, DESY 81-088 (1981).

[14] D. Brandt, CERN-LEP Note 512 (1984).

[15] V. Nys, CERN/LEP - TH/86-34 (1986).

[16] P.B. Wilson, K. Bane and K. Satoh, IEEE Trans. Nucl. Sci. **NS-28**, 2525 (1981).

[17] A.G. Ruggiero, IEEE Trans. Nucl. Sci. **NS-24**, 1205 (1977).

[18] E. Keil, PEP Note 126 (1975).

[19] K.L.F. Bane and P.B. Wilson, IEEE Trans. Nucl. Sci. **NS-24**, 1485 (1977).

[20] A.W. Chao and J. Gareyte, Stanford report PEP-224 (1976).

[21] B. Zotter, IEEE Trans. Nucl. Sci. **NS-28**, 2602 (1981).

[22] F. Sacherer, CERN/SI - BR/72-5 (1972).

[23] K. Oide and K. Yokoya, KEK Preprint 90-10 A (1990).

[24] K. Hirata, Particle Accelerators **22**, 57 (1987).

[25] M. Abramovitz, I.A. Stegun, Handbook of Mathematical Functions, Dover, New York (1965), ch. 1.

[26] K. Robinson, CEA-11 (1956) AND CEAL-1010 (1964).

[27] L. Volkovysky, G. Lunts and I. Aramanovich, Problems in the Theory of Functions of a Complex Variable, MIR, Moscow (1972), ch. 4.5.

[28] W.H. Press, B.P. Flannery, S.A. Teukolsky and W.T. Vetterling, Numerical Recipes, Cambridge Univ. Press (1986).

[29] P.B. Wilson, PEP Note 232 (1977).

[30] D. Brandt et al, LEP Commissioning Note 21 (1989).

[31] K. Hirata, CERN/LEP - TH/88-02 (1988).

[32] R.J. Schwarz and B. Friedland, Linear Systems, McGraw–Hill, New York (1965), ch. 12.